Bioorganic Chemistry 38 (2010) 252–259

Contents lists available at ScienceDirect

Bioorganic Chemistry

journal homepage: www.elsevier.com/locate/bioorg

Kinetic and structural characterization of DmpI from *Helicobacter pylori* and *Archaeoglobus fulgidus*, two 4-oxalocrotonate tautomerase family members ☆,☆☆

Jeffrey J. Almrud [a], Rakhi Dasgupta [b], Robert M. Czerwinski [a], Andrew D. Kern [b], Marvin L. Hackert [b,*], Christian P. Whitman [a,**]

[a] Division of Medicinal Chemistry, College of Pharmacy, The University of Texas, Austin, TX 78712-1071, United States
[b] Department of Chemistry and Biochemistry, The University of Texas, Austin, TX 78712-1071, United States

ARTICLE INFO

Article history:
Received 14 June 2010
Available online 18 July 2010

Keywords:
4-oxalocrotonate tautomerase
Catalytic proline
Hexamer

ABSTRACT

The tautomerase superfamily consists of structurally homologous proteins that are characterized by a β-α-β fold and a catalytic amino-terminal proline. 4-Oxalocrotonate tautomerase (4-OT) family members have been identified and categorized into five subfamilies on the basis of multiple sequence alignments and the conservation of key catalytic and structural residues. Representative members from two subfamilies have been cloned, expressed, purified, and subjected to kinetic and structural characterization. The crystal structure of DmpI from *Helicobacter pylori* (HpDmpI), a 4-OT homolog in subfamily 3, has been determined to high resolution (1.8 Å and 2.1 Å) in two different space groups. HpDmpI is a homohexamer with an active site cavity that includes Pro-1, but lacks the equivalent of Arg-11 and Arg-39 found in 4-OT. Instead, the side chain of Lys-36 replaces that of Arg-11 in a manner similar to that observed in the trimeric macrophage migration inhibitory factor (MIF), which is the title protein of another family in the superfamily. The electrostatic surface of the active site is also quite different and suggests that HpDmpI might prefer small, monoacid substrates. A kinetic analysis of the enzyme is consistent with the structural analysis, but a biological role for the enzyme remains elusive. The crystal structure of DmpI from *Archaeoglobus fulgidus* (AfDmpI), a 4-OT homolog in subfamily-4, has been determined to 2.4 Å resolution. AfDmpI is also a homohexamer, with a proposed active site cavity that includes Pro-1, but lacks any other residues that are readily identified as catalytic ones related to 4-OT activity. Indeed, the electrostatic potential of the active site differs significantly in that it is mostly neutral, in contrast to the usual electropositive features found in other 4-OT family members, suggesting that AfDmpI might accommodate hydrophobic substrates. A kinetic analysis has been carried out, but does not provide any clues about the type of reaction the enzyme might catalyze.

1. Introduction

4-Oxalocrotonate tautomerase (4-OT) from *Pseudomonas putida* mt-2 catalyzes the conversion of 2-hydroxy-2,4-hexadienedioate (**1**, Scheme 1), also known as 2-hydroxymuconate, to 2-oxo-3-hexenedioate (**2**) [1–4]. This enzyme-catalyzed reaction is one step in a catabolic pathway encoded by the TOL plasmid [1]. Organisms having this plasmid, such as *P. putida* mt-2, can use benzene, toluene, or xylene isomers as their sole sources of carbon and energy [1].

4-OT has two distinguishing features: a catalytic amino-terminal proline and a short monomeric subunit (62 amino acids) that codes a β-α-β structural motif [3,5–7]. These features are also the defining characteristics of the tautomerase superfamily [8–10]. The tautomerase superfamily is a structurally and mechanistically diverse group of proteins whose members exist as dimers, trimers, and homo- and heterohexamers, and catalyze isomerization, hydration, dehalogenation, and decarboxylation reactions [12–17]. In each of these transformations, Pro-1 functions as a general base or a general

Abbreviations: AfDmpI, DmpI from *Archaeoglobus fulgidus*; CaaD and *cis*-CaaD, *trans*- and *cis*-3-chloroacrylic acid dehalogenase respectively; CHMI, 5-(carboxymethyl)-2-hydroxymuconate isomerase; F_o and F_c, observed and calculated structure factors respectively; HEPES, N-(2-hydroxyethyl)piperazine-N′-2-ethanesulfonic acid; HpDmpI, DmpI from *Helicobacter pylori*; IPTG, isopropyl-β-D-thiogalactoside; Kn, kanamycin; LLG, log-likelihood gain; LB, Luria–Bertani; MIF, macrophage migration inhibitory factor; MSAD, malonate semialdehyde decarboxylase; MPD, 2-methyl-2,4-pentanediol; NCS, non-crystallographic symmetry; 4-OT, 4-oxalocrotonate tautomerase; PPT, phenylpyruvate tautomerase; PEG, polyethylene glycol; PCR, polymerase chain reaction; PDB, Protein Data Bank; rmsd, root-mean-square deviation; SDS–PAGE, sodium dodecyl sulfate–polyacrylamide gel electrophoresis.

☆ This research was supported by the National Institutes of Health Grant GM-41239 (CPW) and the Robert A. Welch Foundation grants F-1219 (MLH) and F-1334 (CPW).

☆☆ The atomic coordinates and structure factors of DmpI from *Helicobacter pylori* ($P2_1$ and $P4_1$ space groups) and *Archaeoglobus fulgidus* have been deposited in the Protein Data Bank as entries 2ORM, 3M21, and 3M20, respectively.

* Corresponding author. Fax: +1 512 471 8696.
** Corresponding authors. Fax: +1 512 232 2606.
E-mail addresses: m.hackert@mail.utexas.edu (M.L. Hackert), whitman@mail.utexas.edu (C.P. Whitman).

0045-2068/$ - see front matter © 2010 Elsevier Inc. All rights reserved.
doi:10.1016/j.bioorg.2010.07.002

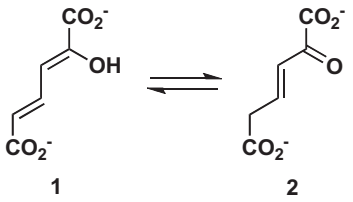

Scheme 1. The 4-OT-catalyzed reaction.

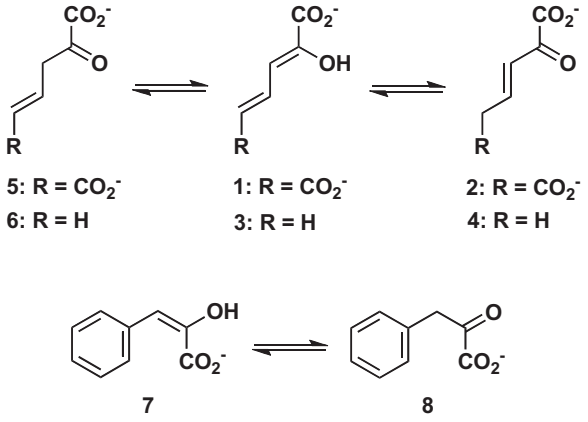

Scheme 2. Substrates processed by HpDmpI and AfDmpI.

acid catalyst [18–21]. In addition, the monomeric subunit consists of a single β-α-β unit or two covalently linked β-α-β units.

Sequence analysis identified several 4-OT homologs in a variety of organisms including the pathogenic bacterium *Helicobacter pylori* and the thermophilic bacterium *Archaeoglobus fulgidus* [12]. In contrast to 4-OT, these homologs are chromosomally encoded, and do not appear to be part of metabolic pathways. Moreover, the host organisms are generally not known to degrade aromatic hydrocarbons.[1] As part of an effort to assign functions for these 4-OT homologs, they were classified into five different subfamilies based on the conservation of key mechanistic and structural residues [12]. DmpI from *H. pylori* and *A. fulgidus* (designated HpDmpI and AfDmpI, respectively) are members of subfamily 3 and 4, respectively. Interestingly, subfamily three members are 4-OT homologs found in bacteria noted for their disease-causing potential, such as *H. pylori*, *Yersinia pestis*, and *Neisseria meningitidis*. Subfamily 4 includes thermophilic bacteria such as *A. fulgidus* and *Methanobacterium thermoautotrophicum*. The DmpI homologs are representative of these two subfamilies and were selected for further characterization.

In this paper, the cloning, overexpression, purification, kinetic characterization, and crystal structures of HpDmpI and AfDmpI are reported. Both enzymes have modest 1,3-keto-enol tautomerase activities converting **1** and 2-hydroxy-2,4-pentadienoate (**3**, Scheme 2) to their β,γ-isomers, **5**, and 2-oxo-4-pentenoate (**6**), respectively, and phenylenolpyruvate (**7**, Scheme 2) to its keto isomer (**8**). The crystal structures show that both enzymes are hexamers where the β-α-β fold is conserved in the monomer. However, the active site pockets differ significantly from those of the other characterized 4-OT family members [4,5,8,12]. The results provide a framework for future studies that might identify biological functions for both proteins and ultimately lead to a better understanding of how diverse functions arose in the tautomerase superfamily.

[1] A recent hypothesis suggests that some 4-OT family members have a regulatory rather than a catalytic biological function. The lack of a metabolic context could be supportive of this hypothesis [Youzhong Guo, PhD Dissertation, The University of Texas at Austin, 2010].

2. Materials and methods

2.1. Materials

All reagents, buffers, and solvents were obtained from Sigma–Aldrich Chemical Co. (St. Louis, MO) unless noted otherwise. The syntheses of 2-hydroxymuconate (**1**, Scheme 1) and 2-hydroxy-2,4-pentadienoate (**3**, Scheme 2) are described elsewhere [2,22]. Isopropyl-β-D-thiogalactoside (IPTG) and thin-walled polymerase chain reaction (PCR) tubes were obtained from Ambion, Inc. (Austin, TX). Bacterial culture media, PCR reagents, molecular biology kits and reagents, oligonucleotide primers, and the bacterial strains used for the construction of the DmpI expression vectors were obtained from the sources listed elsewhere [7,18,23]. The genomic DNA of *H. pylori* strain J99 (ATCC 700824D) and the *A. fulgidus* strain DSM 4304 (ATCC 49558D) was obtained from the American Type Culture Collection (Manassas, VA).

2.2. General methods

Techniques for restriction enzyme digestions, ligation, transformation, and other standard molecular biology manipulations were based on methods described elsewhere [24]. DNA sequencing was done at the University of Texas (Austin) Sequencing Facility. Kinetic data and UV absorbance readings were obtained on a Hewlett Packard 8452A Diode Array spectrophotometer. The kinetic data were fitted by nonlinear regression data analysis using the Grafit program (Erithacus Software Ltd., Staines, UK) obtained from Sigma–Aldrich Chemical Co. High-pressure liquid chromatography was performed on a Waters system using a Bio-Gel Phenyl 5-PW hydrophobic column or a Pharmacia Superose 12 (HR 10/30) gel filtration column. Protein was analyzed by tricine sodium dodecyl sulfate–polyacrylamide gel electrophoresis (SDS–PAGE) under denaturing conditions on 16% gels using a vertical gel electrophoresis apparatus obtained from Bio-Rad (Hercules, CA) [25]. Protein concentrations were determined using the method of Waddell [26]. The electrostatic surfaces of 4-OT, HpDmpI, and AfDmpI were analyzed using the Adaptive Poisson–Boltzmann Solver (APBS) software described elsewhere [27]. The protocol described elsewhere was followed in order to use the APBS software within PyMol [28,29].

2.3. Construction of expression vectors and enzymology methods

2.3.1. Construction of the HpDmpI and AfDmpI expression vectors

The *H. pylori dmpI* gene was amplified from genomic DNA by the PCR using a modification of a procedure described elsewhere [7,23]. Two oligonucleotides, 5′-ACACACACACACCATATGCCGTTTA TCAATATCAAA-3′ (primer-1) and 5′-ACACACACACACGGATCCCTAG TTTTTTTGCCTCAAATG-3′ (primer-2), were synthesized as primers for the PCR. The first primer contains an *Nde*I restriction site (underlined) followed by 18 bases that correspond to the coding sequence of the *H. pylori dmpI* gene. The second primer contains a *BamH*I restriction site (underlined) followed by 21 bases that correspond to the complementary sequence of the *H. pylori dmpI* gene. For the PCR amplification of the *A. fulgidus dmpI* gene, two oligonucleotide primers, 5′-AAGAAGAAGGGATCCCATATGCC AGTCCTGATT GTTTAC-3′ (primer-3) and 5′-TCCAAGCTTGTCGACTTATTCTCGCTCT CTATCCGCTAT-3′ (primer-4), were used. Primer-3 contains an *Nde*I restriction site (underlined) followed by 18 bases corresponding to the coding sequence of the *A. fulgidus dmpI* gene. Primer-4 contains a *Sal*I restriction site (underlined) followed by 24 bases that

correspond to the complementary sequence of the *A. fulgidus dmpI* gene. The additional bases in both sets of primers facilitate DNA cleavage by the restriction enzymes. The PCR was carried out in a Perkin Elmer DNA thermocycler 480 using template DNA, synthetic primers, and the PCR reagents supplied in the PCR Reagent system or the Perkin Elmer Cetus GeneAMP kit following a protocol described elsewhere [7,23]. The resulting gel-purified DNA fragment and the pET24a(+) vector were digested with the appropriate restriction enzymes, purified, and ligated using T4 DNA following a previously described protocol [7,23]. Aliquots of the resulting mixture were transformed into competent *E. coli* JM109 cells and grown on Luria–Bertani plates with kanamycin (Kn) (100 μg/mL) at 37 °C. Single colonies were chosen at random and grown in liquid LB/Kn media (50–100 μg/mL). The newly constructed plasmids containing the *H. pylori* or *A. fulgidus dmpI* genes were isolated and sequenced. Subsequently, the plasmids were transformed as described elsewhere into *E. coli* strain BL21(DE3) pLysS for protein expression [7,23].

2.3.2. Overexpression and purification of the recombinant HpDmpI and AfDmpI

The products of the *H. pylori* and *A. fulgidus dmpI* genes were overexpressed using a previously described protocol [7,23]. Typically, 2 L of culture grown under these conditions yielded 5–7 g of cells. The enzymes were purified to near homogeneity (>95% as assessed by SDS–PAGE) using a combination of the Bio-Gel Phenyl 5-PW hydrophobic column and a Sephadex G-75 gel filtration column (2.5 cm × 100 cm) as described [7,18,23]. Typically, the yield of purified enzyme was 11–16 mg per liter of culture.

2.3.3. Kinetic studies of HpDmpI and AfDmpI

The kinetic studies of HpDmpI and AfDmpI were carried out in 20 mM NaH_2PO_4 buffer, pH 7.3, at 23 °C. The assays were initiated by the addition of varying amounts of **1**, **3**, or **7**. The conversion of **1**–**5**, **1**–**2**, **3**–**6**, and **7**–**8** were monitored as described [12]. For HpDmpI, the substrate and enzyme concentrations were as follows: **1** (5–100 μM, 14 nM); **3** (20–200 μM, 11 nM); and **7** (10–150 μM, 3.4 nM). For AfDmpI, the substrate and enzyme concentrations were as follows: **1** (5–100 μM following **1**–**5** and 30–500 μM following **1**–**2**, 16 nM); **3** (10–200 μM, 8 nM); and **7** (10–150 μM, 8 nM).

2.4. Crystallography methods

2.4.1. Crystallization of HpDmpI and AfDmpI

Crystals of HpDmpI were grown from 28% polyethylene glycol (PEG) 400, 200 mM $CaCl_2$, 0.1 M HEPES buffer (pH 7.5), using Nunc® microplates (Fisher Scientific, Pittsburgh, PA). Protein (3 μL of a 20 mg/mL solution in 50 mM NaH_2PO_4 buffer, pH 7.3) was combined with 3 μL of crystallization solution and then equilibrated by vapor diffusion against 50 μL of well solution at 4 °C. Crystals grew to maturity within 4 days and belong to space group $P2_1$ with cell constants $a = 41.83$ Å, $b = 50.77$ Å, $c = 89.31$ Å and $\beta = 99.1°$. Assuming a hexamer per asymmetric unit, the Matthews coefficient is 2.1 Å^3/Da and corresponds to an approximate solvent content of 42% [30].

Crystals of HpDmpI were also grown from 25% *t*-butanol in 0.1 M sodium citrate buffer, pH 5.5. Protein (5 μL of a 20 mg/mL solution in 50 mM NaH_2PO_4 buffer, pH 7.3) was combined with 5 μL of well solution in a Hampton microbridge (Hampton Research, Aliso Viejo, CA) and equilibrated by vapor diffusion against 500 μL of well solution at 4 °C. Crystals grew to maturity within 6 weeks, and belong to space group $P4_1$ with cell constants $a = b = 53.04$ Å and $c = 130.88$ Å. Assuming a hexamer per asymmetric unit, the Matthews coefficient is 2.08 Å^3/Da, corresponding to an approximate solvent content of 40% [30].

Crystals of AfDmpI were grown from 20% dioxane and 50% 2-methyl-2,4-pentanediol (MPD), pH 6.0. This crystallization condition was prepared by diluting individual stock solutions of 100% dioxane and 100% MPD directly with distilled H_2O. Protein (5 μL of a 15 mg/mL solution in 50 mM HEPES buffer, pH 7.3) was combined with 5 μL of well solution on a Hampton microbridge, and then equilibrated by vapor diffusion against 500 μL of well solution at 4 °C. Crystals belong to the space group $P3_221$, and have cell constants $a = b = 49.1$ Å, $c = 118.8$ Å and $\gamma = 120.0°$. Assuming a trimer in the asymmetric unit, the Matthews coefficient is 2.5 Å^3/Da, and the solvent content is estimated to be 50% [30].

2.4.2. Data collection

Diffraction data of crystals of HpDmpI and AfDmpI were collected using a RAXIS-IV image plate detector installed on a Rigaku RU200H rotating anode X-ray generator. The crystals were mounted in cryo-loops directly from their mother liquor, and flash cooled to −175 °C by immersing the loop directly in liquid nitrogen. Crystals were kept at −165 °C during data collection using a cryo-cooling device (Molecular Structures Corp., The Woodlands, TX). Diffraction data were then processed using the programs DENZO and SCALEPACK [31]. Intensities were converted to structure factors using the program TRUNCATE of the CCP4 suite [32] and R_{free} reflections assigned using the CCP4 program FREERFLAG. The crystal and data collection statistics are summarized in Table 1.

2.4.3. Structure determination and refinement of HpDmpI

For the $P2_1$ data set, the structure of HpDmpI was solved by molecular replacement using a polyalanine search model of 4-oxalocrotonate tautomerase (PDB Accession Code 1-BJP) with B-values set to 40 for all atoms. The cross rotation and translation functions were calculated with the molecular replacement program AMORE [33] using the 30–3 Å resolution data. The correct rotation and translation function solution had a correlation coefficient of 60.3% and an *R*-value of 47.7%. The HpDmpI structure for the $P4_1$ data set was solved using the HpDmpI structure, previously solved in space group $P2_1$ (above) as the search model (B-factors set to 40 for all atoms). The correlation coefficient and *R*-factor for the correct structure were 70.4% and 40.8% respectively.

In both the space groups, the HpDmpI models were refined by iterations of computer-based minimization, followed by manual fitting of the models to electron density maps using the program O [34]. The structure was first refined using REFMAC version 5.0. [35] with a bulk-solvent correction for all rounds of refinement and then refined further using CNSsolve version 1.1 [36]. The decrease in the R_{free} value was used to direct the refinement procedure. Manual rebuilding was carried out using $2F_o–F_c$ electron density maps, with $F_o–F_c$ maps being used to monitor model rebuilding. The HpDmpI model was initially refined with non-crystallographic symmetry (NCS) restraints that were released during later stages of structural refinement. CNSsolve's water-picking routine was used to identify ordered solvent molecules in $F_o–F_c$ electron density maps. After refinement of the protein and solvent model using CNSsolve, the *R* and R_{free} values are 21.7% and 25.3%, respectively for the $P2_1$ space group and 23.6% and 27.7% for the $P4_1$ space group. The refinement statistics are listed in Table 2 and the refined coordinates and structure factors deposited with the Protein Data Bank (PDB) ($P2_1$ space group, 2ORM; $P4_1$ space group, 3M21).

2.4.4. Structure determination and refinement of AfDmpI

The crystal structure of AfDmpI was solved by molecular replacement using a polyalanine search model of 4-OT (PDB Accession Code 1-BJP) with B-values set to 40 for all atoms (as described above). The cross rotation and translation functions were calcu-

Table 1
Crystal and data collection statistics.

	HpDmpI	HpDmpI	AfDmpI
Space group	$P4_1$	$P2_1$	$P3_221$
Cell constants			
a (Å)	53.0	41.8	49.1
b (Å)	53.0	50.8	49.1
c (Å)	130.88	89.3	118.8
α (°)	90.0	90.0	90.0
β (°)	90.0	99.1	90.0
γ (°)	90.0	90.0	120.0
Camera length (mm)	130	130	160
Oscillation angle (°)	2	1.5	2
Exposure time (min)	0.5	20	30
Resolution range (Å)			
Overall	30.0–1.85	25.0–2.10	24.53–2.29
Highest-resolution bin	1.92–1.85	2.18–2.10	2.28–2.20
No. of frames	86	76	39
No. of observations	168,340	120,991	52,778
No. of unique reflections	30,855	21,852	8623
R_{merge} (%)			
Overall	0.044	0.109	0.064
Highest-resolution bin	0.321	0.490	0.407
Completeness (%)			
Overall	89.3	94.3	96.4
Highest-resolution bin	79.9	90.2	85.1
$I/\sigma(I)$	10.3	5.8	14.2

Table 2
Refinement statistics.

	HpDmpI	HpDmpI	AfDmpI
Space group	$P4_1$	$P2_1$	$P3_221$
Refinement resolution range	30.0–1.8	25.0–2.1	24.53–2.37
No. of protein atoms	2923	2969	1270
No. of water molecules	126	273	20
Ramachandran plot			
Residues in core (%)	94.9	96.7	83.8
Residues in allowed region (%)	5.1	3.3	16.2
Deviation in bond distances (Å)	0.005	0.007	0.008
Deviation in bond angles (deg)	0.98	1.13	1.34
B-factor (Å^2)			
Overall	36.5	32.8	46.8
Protein	32.6	28.9	47.0
Solvent	40.3	36.6	48.4
R-factor (%)	23.6	21.7	29.6
R-free (%)	27.7	25.3	31.5

lated with the molecular replacement program BEAST [37] using the 30–3 Å resolution data. The correct rotation and translation function solution had a log-likelihood gain (LLG) score of 164.37. The structure of AfDmpI was refined using the procedures described above for the HpDmpI structure. After refinement, the *R* and R_{free} values were 29.6% and 31.5% respectively. The refinement statistics are listed in Table 2 and the refined coordinates and structure factors deposited with the PDB (3M20).

3. Results

3.1. Kinetic studies of HpDmpI and AfDmpI

Three compounds (**1**, **3**, and **7**, Scheme 2) were examined as potential substrates for HpDmpI and AfDmpI and the steady-state parameters are reported in Tables 3 and 4. HpDmpI has a modest tautomerase activity with these compounds preferring the monocarboxylated substrates (**3** and **7**) to the dicarboxylated substrate **1**, (as indicated by the ~2-fold higher k_{cat}/K_m values) (Table 3). HpDmpI converts **1** to the α,β-isomer (**2**), although the k_{cat}/K_m value is 4300-fold less than that reported for 4-OT [38,39]. While the K_m values are comparable, the k_{cat} for the catalyzed-conversion of **1**–**2** by HpDmpI is about 5800-fold less than that reported for 4-OT [38,39].

Table 3
Kinetic parameters for HpDmpI using **1**, **3**, and **7**[a].

Reaction	k_{cat} (s^{-1})	K_m (μM)	k_{cat}/K_m (M^{-1} s^{-1})
1 → 5	0.6 ± 0.1	110 ± 20	5.4×10^3
3 → 6	2.5 ± 0.3	190 ± 40	1.3×10^4
7 → 8	2.6 ± 0.7	230 ± 90	1.1×10^4
1 → 2	0.6 ± 0.03	135 ± 15	4.4×10^3

[a] The steady-state kinetic parameters were determined in 20 mM sodium phosphate buffer (pH 7.3) at 23 °C. Errors are standard deviations.

Table 4
Kinetic parameters for AfDmpI using **1**, **3**, and **7**[a].

Reaction	k_{cat} (s^{-1})	K_m (μM)	k_{cat}/K_m (M^{-1} s^{-1})
1 → 5	0.2 ± 0.03	170 ± 40	1.2×10^3
3 → 6	0.1 ± 0.02	90 ± 30	1.1×10^3
7 → 8	2.4 ± 0.3	90 ± 20	2.7×10^4
1 → 2	0.05 ± 0.001	110 ± 10	4.5×10^2

[a] The steady-state kinetic parameters were determined in 20 mM sodium phosphate buffer (pH 7.3) at 23 °C. Errors are standard deviations.

AfDmpI also has a modest tautomerase activity with both **1** and **3**, and converts them to their β,γ-unsaturated ketones (**5** and **6**, respectively). AfDmpI will process **1** to the α,β-isomer (**2**), but again, the k_{cat}/K_m value is much lower (42,000-fold) than that reported for 4-OT [38,39]. The K_m values are comparable, but the k_{cat} for catalyzed-conversion of **1**–**2** by AfDmpI is ~70,000-fold less than that reported for 4-OT [38,39]. The most significant AfDmpI activity was observed for the conversion of **7**–**8**, with 22- and 24-fold increases in k_{cat}/K_m relative to those measured respectively for **1** and **3**.

3.2. The crystal structures of HpDmpI

The crystal structure of HpDmpI was determined to 1.8 Å and 2.1 Å resolution in two different space groups ($P2_1$ and $P4_1$). The crystallographic asymmetric unit consists of a hexamer in both

space groups. Electron density for the polypeptide backbone was well ordered for most of the 67 amino acid residues, except for a few C-terminal residues. Residues with missing or poorly defined side chain density were modeled as alanines and reported as such in their respective PDB files. Pro-14 is in the *cis* conformation in all six monomers, and in both space groups. Ramachandran plots for all non-glycine and non-proline residues for the HpDmpI models in the $P2_1$ and $P4_1$ space groups show that 96.7% and 94.9% of the residues lie within the most-favored regions and 3.3% and 5.1% of the residues lie within the additionally allowed regions. For the $P2_1$ space group, the C_a atoms of residues 1–64 in monomer A superimpose with the other five monomers of the same hexamer with an average rmsd value of 0.39 Å (±0.05 Å). The total of twelve, independent HpDmpI monomers for the two structures solved in space groups $P2_1$ and $P4_1$ superimpose with an rmsd value of 0.74 Å.

Like the *P. putida* mt-2 4-OT, the HpDmpI monomer shows the signature β-α-β fold. Accordingly, residues 1–8 comprise a β-strand 1 (β-1), residues 9–15 form a loop connecting β-1 to an α-helix (α-1, residues 16–34), residues 35–37 form a loop that connects α-1 to a 3_{10} helix and turn (38–41 residues). The turn is followed by a second β-strand (β-2, residues 42–47), a loop (residues 48–52), a Type-II β-hairpin (residues 53–59), and ends with a coil conformation (residues 60–67). Within a single monomer, β-1 and β-2 associate in a parallel fashion. The two monomers form a homodimer in such a way that the β-1 and β-2 strands of one monomer run antiparallel with respect to β-1 and β-2 of the second monomer and form a four-stranded β-sheet. HpDmpI hexamer formation is stabilized by dimer-dimer interactions between a strand from the β-hairpin turn from one dimer and an edge of the four-stranded sheet of a second dimer, the result of which is formation of an eight stranded β-sheet involving four subunits.

3.3. The active site of HpDmpI

The active site cavity is presumed to contain Pro-1. The sequence identity with 4-OT and a 4-OT homolog from *Bacillus subtilis* designated YwhB (34% and 28%, respectively) [4,8] was used to identify features and boundaries of the active site cavity. Accordingly, it is proposed that the HpDmpI active site is comprised of residues contributed by the convergence of three monomers (monomer, monomer', and monomer'')[2] at a dimer-dimer interface within the hexamer. One side of the active site is defined by Pro-1, Phe-2, Val-42, and the side chain of Lys-36, whereas the opposite side is defined by Val-42″, Leu-55′, Tyr-53′, and Val-60′ (Fig. 1A). In contrast to 4-OT and YwhB, HpDmpI lacks arginine at position 11. Instead, Pro-14′ (in HpDmpI) diverts the mainchain such that the side chain of Lys-36 is placed with its ε-amino group in the active site (in a nearly equivalent position). Lys-36 is conserved in subfamily-3, and may play a role in binding and/or catalysis (*vide infra*). The architecture of the HpDmpI active site is further defined by the side chain of Tyr-53′, where the phenolic oxygen points into the active site. The floor of the active site floor is formed, in part, by the side chain cluster of Val-8′, Val-48′ (not shown), and Val-60′ on one side of Tyr-53′, and Val-42″ and Ile-44″ (not shown) on the other side of Tyr-53′. The 2-fold molecular symmetry axis relating the two dimers of the hexamer (e.g., Val-42″ to Val-42) generates an adjacent active site (Fig. 1A).

3.4. Structural comparison of HpDmpI with 4-OT

The C_α atoms of residues 1–60 of the 4-OT and HpDmpI monomers superimpose with an rmsd value of ~6.0 Å. The largest differences in the C_α positions are found in loops. The rmsd value between 4-OT and HpDmpI decreases to 0.76 Å if residues corresponding only to the α-helices and β-sheets of a monomer from the two proteins are used in the rmsd calculation.

Although the folds of HpDmpI and 4-OT are highly conserved, the architecture of their active sites is quite different (Figs. 1A, 1C and 2). The key residues in 4-OT have been identified as Pro-1, Arg-11′, Arg-39″, and Phe-50′ [7,8,18,38,39]. Sequence alignments show that Pro-1 is the only conserved residue. Notable differences in the active sites of 4-OT and HpDmpI are observed with the side-chain placements of Arg-11′/Lys-36, Arg-39″/Val-42″, and Phe-50′/Tyr-53′ for these key residues (Fig. 2). Differences are also observed with the side-chain placements of Ile-2/Phe-2, Leu-8′/Val-8′, Ile-52′/Leu-55′, and Ala-57′/Val-60′ (Fig. 2). These differences have an impact on the molecular surface topology and electrostatic potential surface of the HpDmpI active site (Fig. 1B).

The 4-OT active site is bound on opposite ends by residues Arg-11′ and Arg-39″. By the molecular 2-fold axis, Arg-39 has its guanidinium group positioned next to Arg-39″ from an adjacent active site (Fig. 1C). This positioning has two identifiable consequences: the formation of two active sites with clearly defined partitions from its neighboring active site and strong electropositive character at each end of the active site (Fig. 1D). In HpDmpI there is also a clearly defined partition between the proposed two active sites (Fig. 1B). Lys-36 in HpDmpI aligns with Lys-32 of macrophage migration inhibitory factor (MIF) [40], which interacts with a carboxylate oxygen of a substrate (*p*-hydroxyphenylenolpyruvate) for the phenylpyruvate tautomerase (PPT) activity of MIF and an inhibitor [(*E*)-2-fluoro-*p*-hydroxycinnamate)] of the activity. However, HpDmpI lacks Arg-39″, and instead contains a valine (i.e., Val-42″) at the equivalent position. This change results in a loss of electropositive character at one end and an alteration of the surface topology of the active site (Fig. 1B and D).

3.5. The crystal structure of AfDmpI

The crystallographic asymmetric unit of AfDmpI consists of a trimer. The electron density for the polypeptide backbone is well ordered except for residues 60–62 (monomer-A), 58–62 (monomer-B), and 58–62 (monomer-C). In the Ramachandran plot, 83.8% of all non-glycine and non-proline residues lie within the most-favored regions and 16.2% lie within the additionally allowed region. The C_α atoms for monomer A (1–58) and monomer B superimpose with an rmsd of ~0.55 Å and the C_α atoms for monomer A and monomer C superimpose with an rmsd of ~0.59 Å.

Like 4-OT and HpDmpI, the AfDmpI monomer shows the β-α-β fold, but the identities of the residues making up the elements of secondary structure and their lengths are very different. The β-strand 1 (β-1) is made up of residues 1–6 and is followed by a loop (residues 7–12) that connects β-1 to an α-helix (α-1, residues 13–30). A loop (residues 31–37) then connects α-1 to a second β-strand (β-2, residues 38–44), which is followed by a loop (residues 45–48), a Type-II β-hairpin (residues 49–51), and ends with a coil conformation (residues 52–58). β-1 and β-2 associate in a parallel fashion within a single monomer. They then associate to form the hexamer by the antiparallel interaction of β-1 and β-2 of one monomer with β-1 and β-2 of adjacent monomers to form a four-stranded β-sheet. This hexamer is stabilized by dimer-dimer interactions between a strand from the β-hairpin turn from one dimer and an edge of the four-stranded sheet contributed by a second dimer.

3.6. The active site of AfDmpI

Like HpDmpI and all tautomerase superfamily members characterized to date [11], the area around Pro-1 is presumed to be the

[2] The unprimed, primed, and doubly primed residues refer to the different subunits.

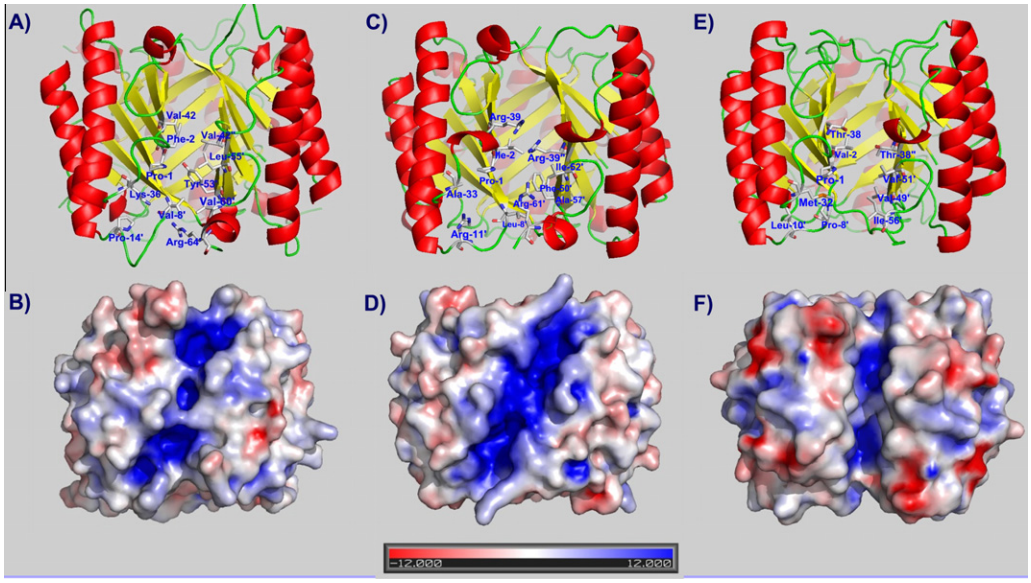

Fig. 1. The proposed active sites and electrostatic surface potentials respectively of A and B) HpDmpI, showing the loss of electropositive character at one end (where Val-42 replaces Arg-39 found in 4-OT, C and D) 4-OT, showing the strong electropositive character at each end of the active site, and E and F) AfDmpI, showing the lack of strong positive or negative electrostatic character. The Adaptive Poisson–Boltzmann Solver (APBS) software was used for evaluating the electrostatic properties [27]. The Figures were prepared with PyMOL using PDB2PQR [28,29].

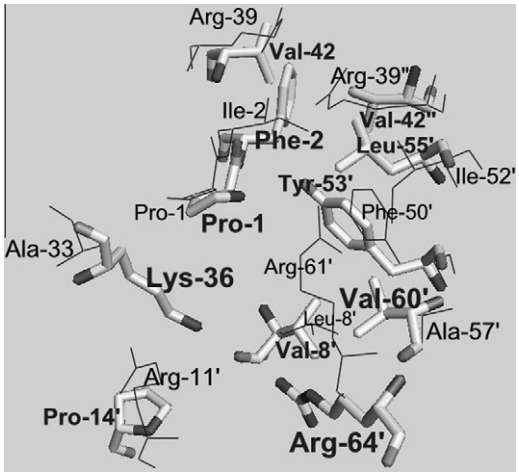

Fig. 2. Superposition of the active site residues of HpDmpI (Pro-1, Lys-36, Val-42″, and Tyr-53′) and the corresponding key catalytic ones in 4-OT (Pro-1, Arg-11′, Arg-39″, and Phe-50′). Arg-64′ is at the entrance of the active site, but has no 4-OT equivalent. The Figure was prepared using PyMol [29].

active site cavity for catalysis, if indeed catalysis is the biological role for this protein.[2] This observation along with sequence alignment between 4-OT and AfDmpI suggest that the active site of AfDmpI could also consist of residues contributed by the convergence of three monomers at a dimer–dimer interface within the hexamer. Hence, it is proposed that one side of the active site is defined by Pro-1, Val-2, Met-32, and Thr-38 whereas the opposite side is defined by Thr-38″, Leu-40″ (not shown), Val-49′, Val-51′, and Ile-56′ (Fig. 1E). The 2-fold molecular symmetry axis relating two dimers of the hexamer (e.g., Thr-38″ to Thr-38) generates an adjacent active site (Fig. 1E).

3.7. Structural comparison of AfDmpI with 4-OT

AfDmpI shares 14% sequence identity with the *P. putida* 4-OT. The C_α atoms (1–59 of 4-OT and 1–59 of the AfDmpI monomer) superimpose with an rmsd of ~3.66 Å where the largest positional differences are again observed in the various loops. The rmsd between 4-OT and AfDmpI decreases to 0.60 Å if the C_α atom positions corresponding to only the monomer's β-sheets are calculated from the superposition.

The architecture of the 4-OT and AfDmpI active sites is strikingly different. AfDmpI retains the critical structural residues (e.g., Lys-16, Glu-44 or Asp-44, Gly-54, and an aromatic residue, i.e., Tyr, in the Phe-50 position, using the 4-OT numbering system). Pro-1 is conserved, but AfDmpI does not conserve any other active site residues (Fig. 3). Differences in the architecture of the active sites of 4-OT and AfDmpI are especially evident in the side-chain placements of Arg-11′/(side chain of) Met-32, Arg-39″/Thr-38″, Ile-52′/Val-51′, Ala-57′/Ile-56′, and Phe-50′/Val-49′ (Fig. 3). These

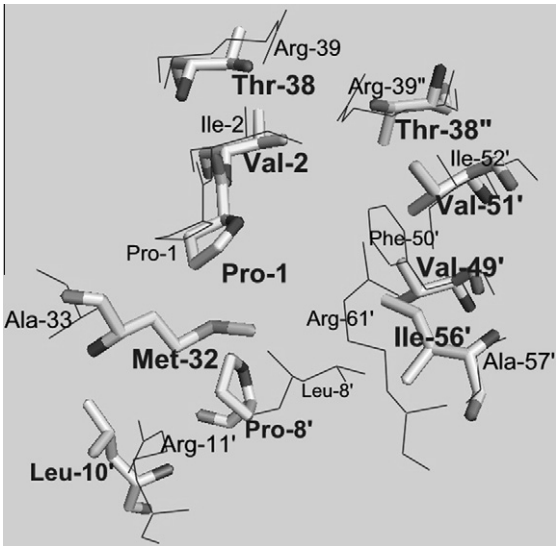

Fig. 3. Superposition of the proposed active site residues of AfDmpI (Pro-1, Met-32, Thr-38″, and Val-49′) and the corresponding key catalytic ones in 4-OT (Pro-1, Arg-11′, Arg-39″, and Phe-50′). The figure was prepared using PyMol [29].

differences have an impact on the molecular surface topology and electrostatic potential surface of the AfDmpI active site (Fig. 1D and F). The lack of both Arg-11′ and Arg-39″, with methionine (i.e., Met-32) and threonine (i.e., Thr-38″) at the equivalent positions results in a calculated surface topology for the AfDmpI active site as an elongated and hydrophobic cavity with an overall lack of positive (or negative) electrostatic character (Fig. 1F).

4. Discussion

Thus far, the tautomerase superfamily consists of five families [8–10]. The title enzymes of the three founding families of the superfamily are 4-OT, a bacterial isomerase known as 5-(carboxymethyl)-2-hydroxymuconate isomerase (CHMI), and a mammalian cytokine, macrophage migration inhibitory factor (MIF), which has a PPT activity [8,9]. Two additional families were uncovered in the course of the characterization of a bacterial catabolic pathway for 1,3-dichloropropene [11]. The isomeric mixture of 1,3-dichloropropene is converted (in three enzymatic steps) to the *cis*- and *trans*-isomers of 3-chloroacrylate, which, in turn, are processed by isomer-specific dehalogenases (*cis*- and *trans*-3-chloroacrylate dehalogenase designated *cis*-CaaD and CaaD, respectively) to malonate semialdehyde. Decarboxylation of malonate semialdehyde by malonate semialdehyde decarboxylase (MSAD) yields acetaldehyde, which is likely routed to the Krebs cycle. MSAD and *cis*-CaaD represent separate families in the tautomerase superfamily. CaaD, and the 4-OT homologs designated YwhB and YdcE, are 4-OT family members. All of these enzymes have the characteristic β-α-β building block and Pro-1, which functions as a catalytic base (4-OT, CHMI, PPT activity of MIF, YdcE, YwhB) or acid (CaaD, *cis*-CaaD, MSAD) [4,8–10,12,23].

In 2002, thirty-seven 4-OT homologs (including CaaD) were identified and categorized into five subfamilies, based on the conservation of key structural and catalytic residues [12]. With the results of this study, members from all five subfamilies have now been expressed and their properties characterized. 4-OT and YwhB are members of subfamilies 1 and 2, respectively [12]. HpDmpI is a member of subfamily 3, and AfDmpI and both the α- and β-subunits of CaaD are members of subfamily 4. YdcE, a homolog from *E. coli*, is found in subfamily 5. All five homologs function as tautomerases with varying efficiencies.[3] Since 2002, the number of sequences annotated as 4-OT homologs has increased considerably, but biological functions for these as well as many of the thirty-seven original 4-OT homologs have yet to be determined.

This sequence analysis coupled with structural and biochemical characterization provide significant insight into the structures and mechanisms of the 4-OT homologs, and the roles played by the conserved residues. The proteins in subfamilies 1–4 conserve four structural residues, (Lys-16, Glu-44, Phe-50, and Gly-54, using the 4-OT numbering system), whereas subfamily 5 members do not [12]. Consequently, members of subfamilies 1–4 form hexamers (or a heterohexamer, in the case of CaaD) and those in subfamily 5 form dimers. In 4-OT, hexamer formation is governed by presence of Phe-50 and Gly-54. Gly-54 is at the end of a β-hairpin sequence (GXGG) that follows the aromatic amino acid and produces a tight turn [5,12]. The hairpin interacts with, and extends the β-sheet of an adjacent 4-OT dimer. In this way, the β-hairpin stabilizes adjacent dimers in the hexamer. The same motif is found in HpDmpI (i.e., a tyrosine residue followed by GLGG) and AfDmpI (a valine residue followed by GVGG), and structural analysis confirms that HpDmpI and AfDmpI are both hexamers. YdcE from *E. coli* and XF1725 from *Xylella fastidiosa* (both in subfamily 5) lack the β-hairpin sequence following the aromatic residue [12]. The β-hairpin sequence and the eight following residues in 4-OT are replaced with 26 residues in YdcE. These residues (forming an α-helix, a π-helix, and another α-helix) take the place of the adjacent dimers in 4-OT in that the helical region fills in the space occupied by the adjacent dimers in 4-OT. The aromatic amino acid, Phe-50 in 4-OT, plays an additional role: it creates a local hydrophobic region near Pro-1 that may play a role in lowering the pK_a of Pro-1 to 6.4 [18].

In addition to these structural elements, the members of subfamily-1 conserve three catalytic residues, Pro-1, Arg-11′, and Arg-39″. In 4-OT, Pro-1 has a pK_a of ∼6.4, and functions as a base that transfers the 2-hydroxy proton of **1** to C-5 of **2** with a high degree of stereoselectivity [4,6,7]. Arg-11′ binds the C-6 carboxylate group of **1** and may also function as an electron sink to draw electron density to C-5, thereby facilitating protonation [38,39]. Arg-39″ interacts with a carboxylate oxygen of C-1, serving as one binding determinant, and may stabilize the developing carbanionic character of the intermediate after deprotonation of the 2-hydroxy group [11,38,39].

In subfamily 2, Arg-39 is replaced with a histidine except in YwhB, where it is replaced with a valine. YwhB is an efficient 1,3-keto-enol tautomerase (converting **1**, **3**, and **7** respectively to **5**, **6**, and **8**) in contrast to 4-OT, which is a highly efficient 1,5-keto-enol tautomerase (using **1**, for example) [4]. YwhB also processes **1**–**2**, but the k_{cat}/K_m value is down ∼680-fold. Both the YwhB-catalyzed 1,3- and 1,5-keto-enol tautomerase activities are dependent on Pro-1 and Arg-11. However, changing Arg-11 to an alanine is much more detrimental to these activities than changing Pro-1 to an alanine.

These observations and the stereochemical findings (using mono- and dicarboxylated substrates) suggest that the mechanism of YwhB parallels that of 4-OT [4,23]. Accordingly, Pro-1 likely has a low pK_a (∼6.4) and functions as a base [4,23]. The mono- and diacids bind in different orientations: the C-1 carboxylate group of a monoacid substrate interacts with Arg-11′ whereas the C-6 carboxylate group of the diacid substrate interacts with Arg-11′. In this orientation, the C-1 carboxylate group interacts with an unknown residue. As noted above, YwhB has valine in place of the 4-OT Arg-39 whereas the other subfamily-2 members have a histidine. It is not yet known how the presence of this charged residue will affect the 1,3- and 1,5-keto-enol tautomerase activities (assuming these are the major activities identified for the other subfamily members).

Subfamily-3 members, such as HpDmpI, lack both Arg-11 and Arg-39 (or equivalent residues). However, this group contains a conserved lysine (Lys-36 in HpDmpI) that aligns with Lys-32 of MIF. Crystallographic studies implicated Lys-32 in the binding of a substrate (i.e., *p*-hydroxyphenylenolpyruvate) for the PPT activity of MIF as well as in the binding of an inhibitor, (*E*)-2-fluoro-*p*-hydroxycinnamate [40,42]. In both cases, an interaction is observed between the oxygen of the C-1 carboxylate group and Lys-32 [40,42]. However, changing Lys-32 to an alanine has little effect on the PPT activity of MIF [43]. Moreover, the K32A mutant is highly stereoselective, (comparable to that of wild type), when the reaction is carried out in D_2O [43]. There is a change in the K_i value for (*E*)-2-fluoro-*p*-hydroxycinnamate and the K32A mutant, but only an 15-fold increase (2.6–40 mM) [43]. Based on these observations, Lys-32 is not a significant determinant in the binding of this substrate or inhibitor.

Lys-32 in MIF may also be one factor responsible for the low pK_a of Pro-1 (∼5.6) [42]. Pro-1 is located in a hydrophobic cleft where it is proximal to Lys-66 and Lys-32 [42]. Mutation of Lys-32 to an alanine significantly raises the pK_a of Pro-1 (∼1.3 units) in a pH rate profile, suggesting that the primary function of Lys-32 is to lower the pK_a of Pro-1 [40]. Based on these observations, the combination of the aromatic amino acid (tyrosine) preceding the β-hairpin se-

[3] CaaD, a member of subfamily 4, has a robust PPT activity, converting 7–8 [41].

quence (GLGG) and Lys-36 (in HpDmpI) may contribute to the presumed low pK_a of Pro-1. The substrate for HpDmpI may be a monoacid and a binding role for Lys-36 cannot be excluded.

Interestingly, 4-OT and YwhB show a low level CaaD activity [8]. In both cases, Pro-1 is critical for the activity. Arg-11 is critical for the CaaD activity of YwhB but has no detrimental effect on that of 4-OT. (In fact, the activity increases slightly in the R11A mutant of 4-OT.) It is not known if subfamilies 3–5 members have low level CaaD activities (or other low level activities). The characterization of YwhB provided significant insight into the reaction and mechanism of 4-OT. Likewise, characterization of the activities of these other 4-OT homologs may provide clues about other activities and chart an evolutionary trail.

Subfamily-4 is the least understood of the five subfamilies because the characteristics are not well defined. Other than the N-terminal proline, the amino acid sequence comparisons do not identify any common active site residues (except for CaaD) [13,19]. The catalytic arginine residues found in 4-OT are replaced by valines. The calculated surface topology for AfDmpI suggests that the active site is a deep and well-defined cavity devoid of positive (or negative) electrostatic patches, and varies significantly from that of 4-OT and HpDmpI.

Initial enzymatic characterization of AfDmpI appears to support our interpretation of the chemical dissimilarity between AfDmpI and 4-OT, and the 4-OT homologs characterized to date. AfDmpI prefers monocarboxylate substrates with the non-carboxylate end of the molecule being hydrophobic in nature, which is consistent with the identification of **7** as the best substrate screened in our studies. This observation is also in agreement with our crystallographic observation that the ends of the AfDmpI active site are hydrophobic in character where the arginine residues are replaced with valines. It is unclear which group, if any, interacts with the C-1 carboxylate. The true substrate may not be a mono- or diacid substrate, but an enol wedged between hydrophobic groups. The future characterization of members of this subfamily should provide better understanding of substrate preferences and architectural functionality of the proteins' active sites.

Acknowledgment

The authors thank Dr. Youzhong Guo (The University of Texas at Austin) for helpful comments and technical support of this project.

References

[1] S. Harayama, P.R. Lehrbach, K.N. Timmis, J. Bacteriol. 160 (1984) 251–255.
[2] C.P. Whitman, B.A. Aird, W.R. Gillespie, N.J. Stolowich, J. Am. Chem. Soc. 113 (1991) 3154–3162.
[3] L.H. Chen, G.L. Kenyon, F. Curtin, S. Harayama, M.E. Bembenek, G. Hajipour, C.P. Whitman, J. Biol. Chem. 267 (1992) 17716–17721.
[4] S.C. Wang, W.H. Johnson Jr., R.M. Czerwinski, S.L. Stamps, C.P. Whitman, Biochemistry 46 (2007) 11919–11929.
[5] H.S. Subramanya, D.I. Roper, Z. Dauter, E.J. Dodson, G.J. Davies, K.S. Wilson, D.B. Wigley, Biochemistry 35 (1996) 792–802.
[6] J.T. Stivers, C. Abeygunawardana, A.S. Mildvan, G. Hajipour, C.P. Whitman, L.H. Chen, Biochemistry 35 (1996) 803–813.
[7] R.M. Czerwinski, W.H. Johnson Jr., C.P. Whitman, T.K. Harris, C. Abeygunawardana, A.S. Mildvan, Biochemistry 36 (1997) 14551–14560.
[8] C.P. Whitman, Arch. Biochem. Biophys. 402 (2002) 1–13.
[9] A.G. Murzin, Curr. Opin. Struct. Biol. 6 (1996) 386–394.
[10] G.J. Poelarends, C.P. Whitman, Bioorg. Chem. 32 (2004) 376–392.
[11] G.J. Poelarends, V.P. Veetil, C.P. Whitman, Cell Mol. Life Sci. 65 (2008) 3606–3618.
[12] J.J. Almrud, A.D. Kern, S.C. Wang, R.M. Czerwinski, W.H. Johnson Jr., A.G. Murzin, M.L. Hackert, C.P. Whitman, Biochemistry 41 (2002) 12010–12024.
[13] G.J. Poelarends, R. Saunier, D.B. Janssen, J. Bacteriol. 183 (2001) 4269–4277.
[14] S.C. Wang, M.D. Person, W.H. Johnson Jr., C.P. Whitman, Biochemistry 42 (2003) 8762–8773.
[15] G.J. Poelarends, H. Serrano, M.D. Person, W.H. Johnson Jr., A.G. Murzin, C.P. Whitman, Biochemistry 43 (2004) 759–772.
[16] G.J. Poelarends, W.H. Johnson Jr., A.G. Murzin, C.P. Whitman, J. Biol. Chem. 278 (2003) 48674–48683.
[17] J.J. Almrud, G.J. Poelarends, W.H. Johnson Jr., H. Serrano, M.L. Hackert, C.P. Whitman, Biochemistry 44 (2005) 14818–14827.
[18] R.M. Czerwinski, T.K. Harris, M.A. Massiah, A.S. Mildvan, C.P. Whitman, Biochemistry 40 (2001) 1984–1995.
[19] R.M. de Jong, W. Brugman, G.J. Poelarends, C.P. Whitman, B.W. Dijkstra, J. Biol. Chem. 279 (2004) 11546–11552.
[20] H.F. Azurmendi, S.C. Wang, M.A. Massiah, G.J. Poelarends, C.P. Whitman, A.S. Mildvan, Biochemistry 43 (2004) 4082–4091.
[21] G.J. Poelarends, H. Serrano, W.H. Johnson Jr., D.W. Hoffman, C.P. Whitman, J. Am. Chem. Soc. 126 (2004) 15658–15659.
[22] H. Lian, C.P. Whitman, J. Am. Chem. Soc. 115 (1993) 7978–7984.
[23] S.C. Wang, W.H. Johnson Jr., R.M. Czerwinski, C.P. Whitman, Biochemistry 43 (2004) 748–758.
[24] J. Sambrook, E.F. Fritsch, T. Maniatis, Molecular Cloning: A Laboratory Manual, Cold Spring Harbor Laboratory, Cold Spring Harbor, New York, 1989.
[25] U.K. Laemmli, Nature 227 (1970) 680–685.
[26] W.J. Waddell, J. Lab. Clin. Med. 48 (1956) 311–314.
[27] N.A. Baker, D. Sept, S. Joseph, M.J. Holst, J.A. McCammon, Proc. Natl. Acad. Sci. USA 98 (2001) 10037–10041.
[28] T.J. Dolinsky, J.E. Nielsen, J.A. McCammon, N.A. Baker, Nucleic Acids Res. 32 (2004) W665–W667.
[29] W.L. DeLano, The PyMOL molecular Graphics System, DeLano Scientific, San Carlos, CA, 2002. <http://www.pymol.org>.
[30] B.W. Matthews, J. Mol. Biol. 33 (1968) 491–497.
[31] Z. Otwinowski, W. Minor, in: C.W. Carter Jr., R.M. Sweet (Eds.), Methods in Enzymology, vol. 276, Academic Press, New York, 1997, pp. 307–326.
[32] Collaborative Computational Project, Number 4. (1994) Acta Crystallogr. D 50 (1994) 760-763.
[33] J. Navaza, Acta Crystallogr. A 50 (1994) 157–163.
[34] T.A. Jones, J.-Y. Zou, S.W. Cowan, M. Kjeldgaard, Acta Crystallogr. A 47 (1991) 110–119.
[35] G.N. Murshudov, A.A. Vagin, E.J. Dodson, Acta Crystallogr. D 53 (1997) 240–255.
[36] A.T. Brünger, P.D. Adams, G.M. Clore, W.L. DeLano, P. Gros, R.W. Grosse-Kunstleve, J.-S. Jiang, J. Kuszewski, M. Nilges, N.S. Pannu, R.J. Read, L.M. Rice, T. Simonson, G.L. Warren, Acta Crystallogr. D 54 (1998) 905–921.
[37] R.J. Read, Acta Crystallogr. Biol Crystallogr. D 57 (2001) 1373–1382.
[38] R.M. Czerwinski, T.K. Harris, W.H. Johnson Jr., P.M. Legler, J.T. Stivers, A.S. Mildvan, C.P. Whitman, Biochemistry 38 (1999) 12358–12372.
[39] T.K. Harris, R.M. Czerwinski, W.H. Johnson Jr., P.M. Legler, C. Abeygunawardana, M.A. Massiah, J.T. Stivers, C.P. Whitman, A.S. Mildvan, Biochemistry 38 (1999) 12343–12357.
[40] A.B. Taylor, W.H. Johnson Jr., R.M. Czerwinski, H.S. Li, M.L. Hackert, C.P. Whitman, Biochemistry 23 (1999) 7444–7452.
[41] G.J. Poelarends, W.H. Johnson Jr., H. Serrano, C.P. Whitman, Biochemistry 46 (2007) 9596–9604.
[42] J.B. Lubetsky, M. Swope, C. Dealwis, P. Blake, E. Lolis, Biochemistry 38 (1999) 7346–7354.
[43] W.H. Johnson Jr., R.M. Czerwinski, S.L. Stamps, C.P. Whitman, Biochemistry 38 (1999) 16024–16033.